Available online at www.sciencedirect.com
ScienceDirect
Journal of Power Sources 174 (2007) 237–245
JOURNAL OF POWER SOURCES
www.elsevier.com/locate/jpowsour

Significant impact of nitric acid treatment on the cathode performance of $Ba_{0.5}Sr_{0.5}Co_{0.8}Fe_{0.2}O_{3-\delta}$ perovskite oxide via combined EDTA–citric complexing process

Wei Zhou, Ran Ran, Zong Ping Shao *, Hong Xia Gu, Wan Qin Jin, Nan Ping Xu

College of Chemistry and Chemical Engineering, Nanjing University of Technology, No. 5 Xin Mofan Road, Nanjing 210009, Jiangsu, PR China

Received 18 April 2007; received in revised form 18 August 2007; accepted 30 August 2007
Available online 4 September 2007

Abstract

$Ba_{0.5}Sr_{0.5}Co_{0.8}Fe_{0.2}O_{3-\delta}$ (BSCF) perovskite was synthesized by the sol–gel process based on EDTA–citrate (EC) complexing method, nitric acid modified EC route (NEC) and nitric acid aided EDTA–citrate combustion process (NECC). A crystallite size of 27, 38 and 42 nm, respectively, was observed for the powders of NECC-BSCF, NEC-BSCF and EC-BSCF calcined at 1000 °C, suggesting the suppression effect of nitric acid on the crystallite size growth of BSCF. The smaller crystallite size of the powders resulted in the higher degree of sintering of the cathode. Oxygen permeation study of the corresponding membranes demonstrated that in the powder synthesis, nitric acid also had a noticeable detrimental effect on the oxygen surface exchange kinetics and on the oxygen bulk diffusion rate of the BSCF oxides. The effect of powder synthesis route on the bulk properties of the oxide was validated by the oxygen temperature-programmed desorption technique. On the whole, a decreasing cathode performance in the sequence of EC-BSCF, NEC-BSCF and NECC-BSCF was observed. A peak power density of 693 mW cm^{-2} was achieved for an anode-supported cell with an EC-BSCF cathode at 600 °C, which was significantly higher than that with an NEC-BSCF cathode (571 mW cm^{-2}) or an NECC-BSCF cathode (543 mW cm^{-2}) under similar operation conditions.

Keywords: $Ba_{0.5}Sr_{0.5}Co_{0.8}Fe_{0.2}O_{3-\delta}$; Synthesis; Solid-oxide fuel cell; Perovskite; Electrical conductivity

1. Introduction

Solid-oxide fuel cells (SOFCs) are a promising power generation technology characterized by high energy conversion efficiency and low pollutant emission. Traditional SOFCs are based on thick YSZ electrolyte membrane and operate at typically 1000 °C [1,2]. However, such high operating temperatures may result in a fast degradation of fuel cell performance due to the increased phase reaction between cell components and the easy sintering of the electrode. Therefore, it is a general trend for SOFCs to operate at reduced temperatures (<800 °C) [3–9]. Unfortunately the reduction of oxygen is a process requiring high activation energy, so that the decrease in operating temperature leads to a sharp increase in cathode polarization resistance of the traditional $La_{1-x}Sr_xMnO_{3-\delta}$ cathodes. The improvement of cathode performance is therefore critical for SOFC technology at reduced temperatures.

Considerable efforts have been devoted to decrease the cathode polarization at reduced temperatures [10–20]. One strategy is to develop new cathode materials with mixed oxygen ionic and electronic conductivity [10–16]. Such materials extend the oxygen reduction site from the traditional triple-phase boundary (cathode–electrolyte–gas phase) to the entire cathode–gas phase interface; therefore, a substantial increase in the cathode performance at reduced temperatures could be observed. On the other hand, cathode performance was also found closely related to the cathode architecture. The development of novel fabrication techniques that can promote gas diffusion and maximize the cathode area for oxygen reduction has also received great attention [17–20].

The cathode layer in SOFCs is usually fabricated with pre-crystallized powders by any of the methods including spray deposition, screen-printing or painting techniques, followed by high temperature sintering. Many powder synthesis meth-

* Corresponding author. Tel.: +86 25 83587722; fax: +86 25 83365813.
E-mail address: shaozp@njut.edu.cn (Z.P. Shao).

0378-7753/$ – see front matter © 2007 Elsevier B.V. All rights reserved.
doi:10.1016/j.jpowsour.2007.08.087

ods have been applied to the synthesis of cathode materials, such as solid-state reaction, sol–gel, co-precipitation, hydrothermal synthesis, etc. [21–25]. Many researches have shown that synthesis methods may affect the morphology, conductivity, crystallite size and surface microstructure of the derived powders [26–30]. Such distinctions could have an evident influence on their properties in applications such as separation membrane and cathode for SOFCs. Indeed, it has been reported that powder synthesis methods had significant effects on the oxygen permeability of ceramic membranes based on mixed-conducting perovskite [28,30–32]. Establishing the relationship between the powder synthesis route and the cathode properties is therefore important for the improvement of the cathode performance. However, systematic reports about the effect of powder synthesis technique on cathode performance of SOFCs [29] are very rare.

Shao et al. first reported $Ba_{0.5}Sr_{0.5}Co_{0.8}Fe_{0.2}O_{3-\delta}$ (BSCF) mixed-conducting perovskite oxide as a potential cathode for intermediate temperature solid-oxide fuel cells (IT-SOFCs) [33]. The application of this material in IT-SOFCs has since received considerable attention [34–40]. In this study, the BSCF perovskite was selected for the demonstration of the significant effect of powder synthesis route on cathode performance. In our previous study, we found that the combined EDTA–citrate (EC) complexing method was effective to synthesize nanocrystalline composite oxides [41]. The addition of nitric acid during the EC complexing process could improve the catalytic activity of $La_{0.6}Sr_{0.4}Co_{0.2}Fe_{0.8}O_{3-\delta}$ composite oxide [42] and depress the crystallite size of the BSCF composite oxide [43]. Therefore, the nitric acid modified EDTA–citrate (NEC) route and the nitric acid aided EDTA–citrate combustion (NECC) process were selected to compare with the EC complexing method.

2. Experimental

2.1. Synthesis of BSCF powders

All the three synthesis routes started from the same EDTA–citrate–metal precursor with a preparation procedure similar to our previous reports [41]. Appropriate amounts of metal nitrates were dissolved in water to make a mixed solution followed by the addition of EDTA and citric acid, which served as the complexing agents. Mild heating induced the gelation of the solution. The gels thus obtained were pre-heated at 250 °C for 5 h to form solid precursors. For the combined EDTA–citrate complexing method, the solid precursor was directly calcined in stagnant air at 1000 °C or 5 h. As for the nitric acid modified EDTA–citrate and the nitric acid modified EDTA–citrate combustion routes, for preparing 0.01 mol BSCF, an amount of 10 ml (NEC) or 30 ml (NECC) concentrated nitric acid (67 wt.%) was dropped into the solid precursor to form a sticky gel, which was then re-heated at 250 °C for 5 h. After the heat treatment, the sample in the 10 ml case converted to a solid precursor, while the one in the 30 ml case resulted in an auto-combustion. Both precursors were then calcined in stagnant air at high temperatures for 5 h to obtain the final products.

2.2. Cell fabrication

Symmetrical cells with the configuration of electrode|SDC|electrode were used for the impedance studies. Dense SDC pellets of 12 mm in diameter and 0.8 mm in thickness were prepared by dry pressing and sintered in air at 1450 °C for 5 h. BSCF powders were first dispersed in a mixed solution of glycerol, ethyleneglycol and isopropyl alcohol to form a colloidal suspension by milling with the help of an agate mortar and pestle. The obtained slurries were painted symmetrically on both surfaces of the SDC pellets, followed by calcination at 1000 °C for 2 h in stagnant air. Silver paste was painted onto the electrode surfaces as current collector.

Anode-supported cells with SDC electrolyte were prepared using a co-pressing technique. Anode powders consisting of 60 wt.% NiO and 40 wt.% SDC were prepared by mixing NiO and SDC in an agate mortar. To fabricate the single cell, the well-mixed NiO–SDC powder was firstly pressed as a substrate, onto which the SDC powder was added and pressed again to form a bilayer pellet. The pellet was then sintered in stagnant air at 1450 °C for 5 h for the densification of the electrolyte layer; the BSCF slurry was painted onto the central surface of the electrolyte and fired at 1000 °C for 2 h in air. The resulting coin-shaped cathode had a thickness of 20 μm and an effective area of 0.52 cm^2.

2.3. Characterization

I–V polarization curves were collected using a Keithley 2420 source meter based on the four-probe configuration. Humidified H_2 (3% H_2O) at a flow rate of 80 ml min^{-1} [STP] was fed into the anode chamber as fuel and compressed air was fed into the cathode chamber as oxidant. Gas flow rates were controlled by mass flow controllers. Silver paste was adopted as current collector.

The electrode performance was investigated with a symmetrical cell or complete cell configuration by the ac impedance method using an electrochemical workstation Solartron 1287 potentiostat and a 1260 A frequency response analyzer. The test was conducted under open circuit voltage (OCV) condition with the frequency ranging from 0.01 to 100 kHz and a signal amplitude of 10 mV. The overall impedance data was fitted by a complex non-linear least square (CNLS) fitting program Z-View 2.9b.

The crystal structure of the synthesized powders was determined by X-ray diffraction (XRD, Bruker D8 Advance) using Cu Kα radiation. The experimental diffraction patterns were collected at room temperature by step scanning within the range of $20° \leq \theta \leq 80°$. The crystallite size was calculated based on the Scherrer equation from the study of Bragg angle and half bandwidth at the index peak of the (1 1 0) plane for BSCF. The microscopic features of the prepared electrodes were characterized by a field emission scanning electron microscopy (FESEM, LEO1530) equipped with an energy dispersive X-ray (EDX) attachment, or an environmental scanning electron microscopy (ESEM, QUANTA-2000). Four-probe dc electrical conductivity of the oxide was measured over the bar-shaped BSCF samples

sintered at 1000 °C in air with silver applied as the electrodes. The current and the voltage were detected by the Keithley 2420 source meter at an interval of 10 °C in the temperature range of 300–900 °C. Oxygen desorption properties of the powders were studied by the oxygen temperature-programmed desorption technique (O_2-TPD). About 150 mg of BSCF powder was loaded in a quartz tube. The assembly was placed in a single-zone furnace equipped with a temperature controller. Argon was used as the carrier gas with a flow rate of 20 ml min^{-1} [STP]. The temperature was increased from 200 to 1000 °C at the rate of 10 °C min^{-1} and the effluent gases were monitored by the mass spectrometer (Hiden, QIC-20).

The oxygen permeation flux measurements were performed using the gas chromatography (GC) method. Single dense membranes or porous BSCF layer modified membranes were sealed onto the quartz support tubes with silver paste. The sidewall of the membrane disks was also covered with the sealant to avoid radial contribution to the oxygen flux due to electrochemical leakage. Helium was used as the sweep gas at a flow rate of 100 ml min^{-1}. A gas chromatograph (Varian, CP 3800) was used to analyze the outlet gas. The oxygen permeation flux was calculated by

$$J_{O_2}\ (\mathrm{ml\,cm^{-2}\,min^{-1}},\ \ [\mathrm{STP}]) = \left[\frac{C_O - C_N \times 0.21}{0.79(28/32)^{1/2}}\right] \times \frac{F}{S}$$

where C_O and C_N are the measured concentrations of oxygen and nitrogen in the gas on the oxygen-lean side (ml ml^{-1}), respectively; F is the flow rate of the exit gas on the oxygen-lean side (ml min^{-1}), and S is the membrane geometric surface area of the sweep side (cm^2).

3. Results and discussion

The synthesis route was found to have a significant effect on the formation of BSCF perovskite. Among the three synthesis routes, the EC method was found to be the most efficient one for preparing pure-phase nano-crystalline BSCF oxide. A pure-phase BSCF was obtained at a firing temperature as low as 850 °C for the EC method, while the temperature had to be as high as 1000 °C for the NEC and NECC methods. The EC method is characterized by the homogeneous mixing of metal ions on the molecular level; it eliminates the blockage of solid-state diffusion for the formation of BSCF oxide and therefore ensures a low temperature synthesis [41]. As shown in Fig. 1, the solid precursor from the EC method took on an amorphous structure even after being heated at 250 °C for 5 h, which implies that the metal ions were still homogeneously distributed in the organic matrix. However, strong characteristic diffraction peaks for $Ba_{0.5}Sr_{0.5}(NO_3)_2$ appeared in the NEC derived solid precursor, which indicated the destruction of the complex. This agrees well with the fact that the conditional stability constants of Ba and Sr with EDTA at a pH value of <4 are both less than zero, i.e., EDTA was not able to immobilize Ba^{2+} and Sr^{2+} anymore under the nitric acid condition. When more nitric acid was applied, i.e., 30 ml HNO_3 applied to the solid precursor for preparing 0.01 mol BSCF powder, a vigorous self-combustion happened.

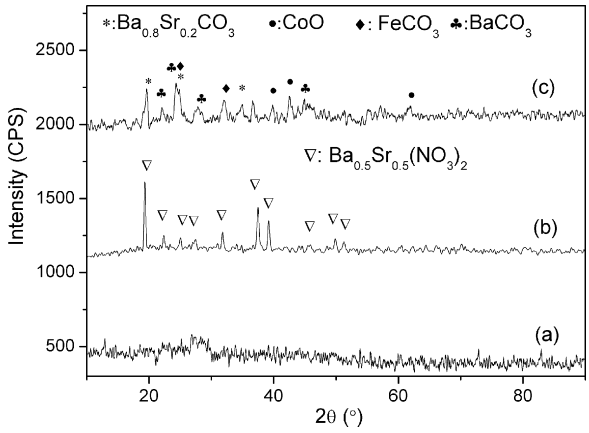

Fig. 1. XRD patterns of three different BSCF solid precursors from different synthesis route methods: (a) EC, (b) NEC and (c) NECC.

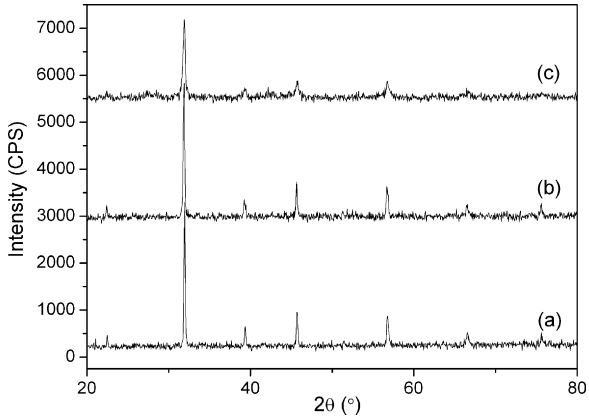

Fig. 2. XRD patterns of three samples calcined at 1000 °C for 5 h: (a) EC-BSCF, (b) NEC-BSCF and (c) NECC-BSCF.

Fig. 2 shows the XRD pattern of the BSCF powders prepared by the three different methods after calcination at 1000 °C for 5 h. All the samples displayed phase-pure cubic perovskite structure. However, a decrease in the crystallinity was observed with the increase of nitric acid applied during the synthesis. The calculated crystallite size and lattice constant of the corresponding BSCF powders are listed in Table 1. Obviously, the crystallite size of BSCF was depressed in the presence of nitric acid during the synthesis [43]. However, the lattice constant of BSCF oxide increased with the amount of nitric acid applied during the synthesis, which suggests that the average valences of cobalt and/or iron ions in BSCF were lowered after the nitric acid treatment of the solid precursor.

Fig. 3 shows the SEM images of various as-synthesized BSCF powders calcined at 1000 °C for 5 h. The powders obtained by

Table 1
Crystallite sizes and lattice constants of the three BSCF powders calcined at 1000 °C for 5 h

Samples	Crystallite size (nm)	Lattice constant (Å)
EC-BSCF	42	3.971
NEC-BSCF	38	3.973
NECC-BSCF	27	3.983

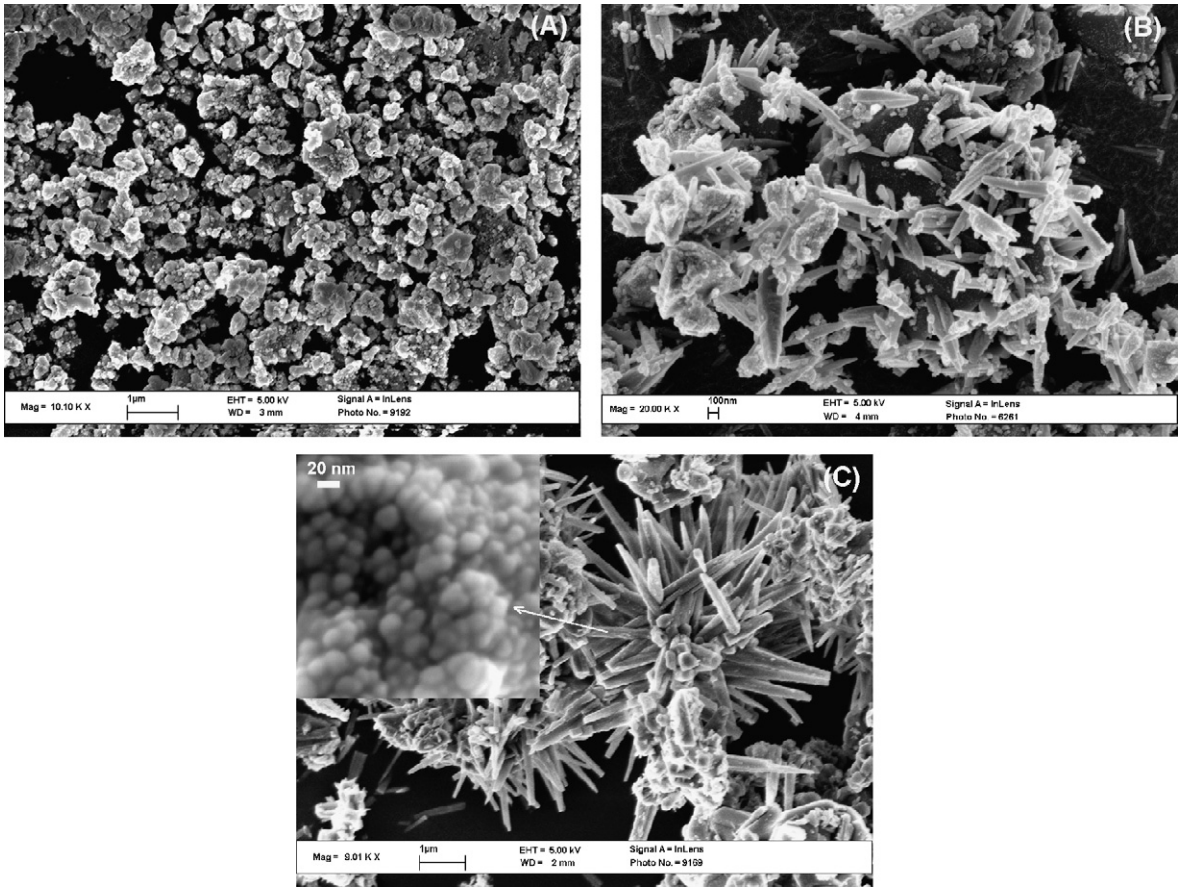

Fig. 3. SEM images of the BSCF powders calcined at 1000 °C for 5 h in air (the inset shows an enlargement of conic BSCF composed of nano-sized particles). (A) EC-BSCF, (B) NEC-BSCF, (C) NECC-BSCF.

the NEC and NECC methods mostly had a conic shape with the grain size varying from several microns to tens of microns. However, the powder prepared by the EC method took on a spherical shape. The relative amount of conic BSCF in the powder increased with the increasing amount of nitric acid applied in the synthesis. The conic particle was actually composed of smaller spherical particles sized 20–40 nm (Fig. 3C), which was comparable to the values reported in other references [44,45]. Subramania et al synthesized nano-crystalline BSCF powders at a temperature as low as 450 °C by a novel sol–gel thermolysis method and the crystallite size of the BSCF provskite oxide was only 34 nm [44]. It should be noted that the temperature for cathode firing process can reach as high as 1000 °C while the BSCF oxide could be easily sintered due to the high surface energy at such a temperature. Therefore, it is more important to prepare nano-crystalline BSCF oxide at higher temperatures in practical use.

The sintering behavior of the various BSCF powders was investigated. Bar-shaped BSCF samples were sintered at 1000 °C for 5 h, and the porosity and shrinkage of samples are shown in Table 2. The relative density of the samples was found to be in the order of EC-BSCF < NEC-BSCF < NECC-BSCF, coinciding with the decreasing crystallite size of the starting powders. Since smaller crystallite size means higher surface energy, higher sintering of ceramics was observed [43]. The effect of the powder preparation method on the electrical conductivity was measured by the four-probe dc method. Fig. 4A shows the temperature dependence of the adjusted conductivity considering the porosity of various BSCF samples measured within the temperature range of 300–900 °C in air. It shows that the electrical conductivity of all samples first increases linearly with temperature to around 450 °C, and then decreases, which can be attributed to the loss of lattice oxygen and the formation of oxygen vacancies at high temperatures (>450 °C). The electrical conductivity increased slightly with the increased amount of nitric acid applied during the synthesis, which might be related to the enhanced contact between neighboring particles.

The electron conducting mechanism below 450 °C can be attributed to the hopping of p-type small polarons, which are associated with the behavior of triple and tetravalent state of cobalt and iron cations. The charge transfer is thermally activated and its temperature dependence is given by the following

Table 2
Shrinkage and porosity of the three BSCF samples calcined at 1000 °C for 5 h

Samples	Shrinkage (%)	Porosity (%)
EC-BSCF	2.15	17.33
NEC-BSCF	2.45	13.99
NECC-BSCF	4.44	11.37

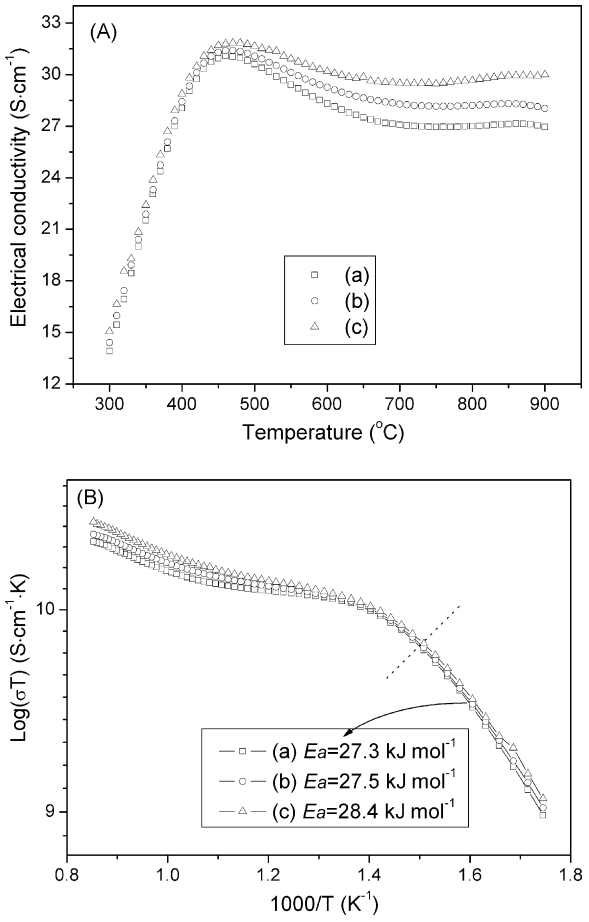

Fig. 4. Electrical conductivity (A) and the corresponding Arrhenius plots of electrical conductivity (B) under air, for the materials synthesized by (a) EC, (b) NEC and (c) NECC methods.

equation:

$$\sigma = \frac{A}{T}\exp\left(\frac{-E_a}{kT}\right)$$

where A is a material constant containing the carrier concentration term, T the absolute temperature, E_a the activation energy for small polaron hopping and k is the Boltzmann constant. Plots of $\log(\sigma T)$ versus $1/T$ are constructed for the temperature range, as shown in Fig. 4B. These plots are linear, and from their slopes the apparent activation energies are calculated. Although the apparent activation energy (300–450 °C) for the three samples is very similar, there are still some slight differences, which is a reflection of the small difference in valences of cobalt and iron ions. The slightly high amount of tetravalent cations within B site is beneficial for the charge transfer. The apparent activation energy is the lowest for EC-BSCF, which may indicate that the amount of Co^{4+} and/or Fe^{4+} in EC-BSCF was higher than those in NEC-BSCF and NECC-BSCF. Since Co^{4+}/Fe^{4+} has a smaller ionic radius than Co^{3+}/Fe^{3+}, a smaller lattice constant of EC-BSCF than NEC-BSCF and NECC-BSCF should be observed, which coincides with the XRD results.

The BSCF powders were then fabricated onto the electrolyte surface as the cathode layer by a painting method followed by calcination at 1000 °C for 5 h in air, with the corresponding SEM photos of the cathode layer shown in Fig. 5. All the three samples show similar porous surface morphology. It is interesting that the conic-shaped particles of BSCF with the powders prepared by the NEC and NECC methods totally disappeared in the cathode layer after the fabrication and calcination. An increased degree of sintering for the cathode layer in the order of EC-BSCF, NEC-BSCF and NECC-BSCF was also observed, coinciding with the fact that the crystallite size of the starting powders decreased in the reverse direction. Smaller crystallite size means a higher surface energy and therefore a higher sinterability. For cathodes based on mixed-conducting oxides, their performance is closely related to the effective surface area, the surface exchange kinetics and also the oxygen bulk diffusion rate of the cathode. The increased degree of sintering would have a detrimental effect on the cathode performance.

The cathode performance of the BSCF oxides prepared by the three different methods was first tested by impedance spectroscopy, and symmetric cells composing of SDC electrolyte and BSCF electrodes were built for this purpose. Fig. 6 shows the temperature dependence of the area-specific resistances (ASRs) under the OCV condition. The EC-BSCF cathode shows both the lowest electrode resistance and activation energy. An ASR of 0.10 Ω cm^2 for the EC-BSCF cathode was observed at 600 °C, while it was 0.36 Ω cm^2 for the NECC-BSCF cathode. The activation energy for EC-BSCF is only 104 kJ mol^{-1}, while it is 117 kJ mol^{-1} for NECC-BSCF. All the above results strongly suggest that the powder preparation method has a significant effect on the cathode performance, the reason for which, according to Fig. 5, could be due to the difference in the effective surface area of the cathodes prepared by different synthesis techniques. The increased degree of sintering with the increased amount of nitric acid applied during the synthesis resulted in the decreasing effective cathode area for oxygen reduction, which should account for the observed decrease in cathode performance.

The performance of the mixed-conducting cathode is closely related not only to its effective surface area, but also to its oxygen surface exchange kinetics and bulk diffusion rate. The effect of the powder preparation method on the oxygen surface exchange and bulk diffusion properties was then quantitatively studied by the oxygen permeation method of dense ceramic membranes. Oxygen permeation through a dense mixed-conducting membrane is usually determined by oxygen surface exchange kinetics combined with oxygen bulk diffusion rate. Under the driving force of the oxygen partial pressure gradient across the membrane, an oxygen molecule first adsorbs over the membrane surface on the oxygen-rich side, where it dissociates into oxygen ions and generates electron holes, both of which then migrate through the bulk of the membrane to the other side of the membrane surface, where they recombine into an oxygen molecule; the molecular oxygen over the membrane surface finally desorbs and evolves into the oxygen-lean side atmosphere. Based on the oxygen permeation fluxes at various conditions, the information of oxygen surface exchange kinetics and bulk diffusion rate can be obtained. For the oxygen permeation study, BSCF powders were fabricated into dense ceramic membranes, and the permeation properties were characterized by the GC method. Shown in Fig. 7 is the temperature dependence of oxy-

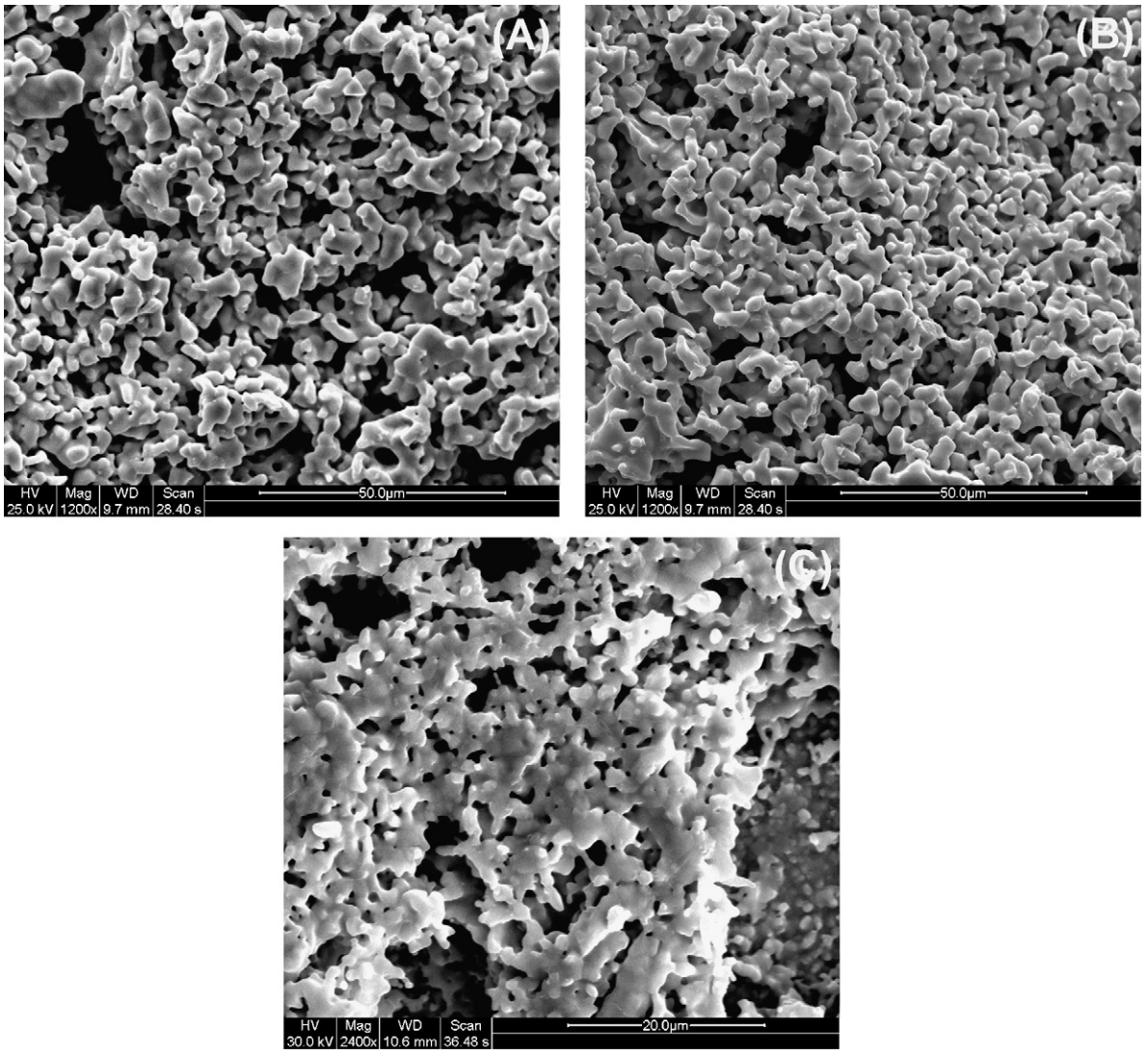

Fig. 5. SEM photos of the 1000 °C calcined cathodes, (A) EC-BSCF, (B) NEC-BSCF and (C) NECC-BSCF.

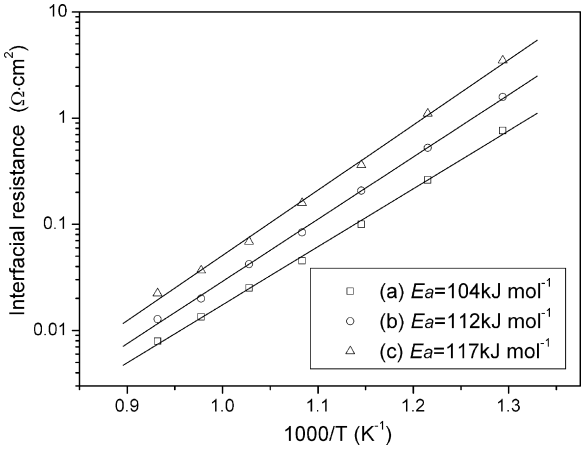

Fig. 6. Arrhenius plots of ASRs for cathode of (a) EC-BSCF, (b) NEC-BSCF and (c) NECC-BSCF.

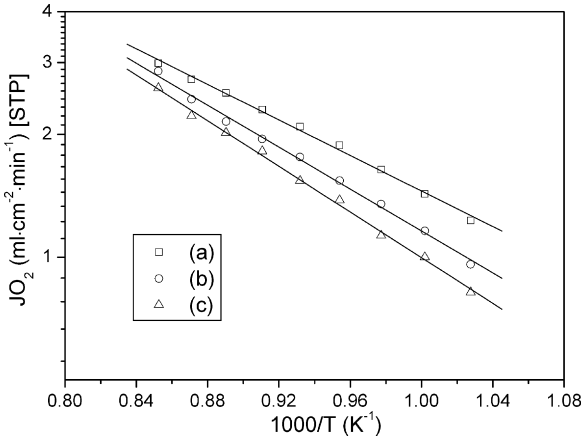

Fig. 7. Arrhenius plots of oxygen permeation fluxes of membranes prepared by (a) EC, (b) NEC and (c) NECC processes. Membrane thickness: 1 mm; He sweep rate: 100 ml min^{-1}.

gen permeation flux through 1.0 mm thick BSCF membranes at a constant helium sweep rate of 100 ml min^{-1} with air being the feed gas. The permeation fluxes were found in the order of EC-BSCF > NEC-BSCF > NECC-BSCF. An increase of the activation energy for oxygen permeation in the sequence of EC-BSCF < NEC-BSCF < NECC-BSCF was also observed. We have shown in a previous paper that the oxygen permeation through surface-unmodified BSCF membrane was mainly rate-determined by the slow oxygen surface exchange kinetics at the oxygen-lean side membrane surface under an air/helium oxygen gradient [46]. It therefore suggests that the increase of nitric acid applied in the powder synthesis led to the decrease of oxygen surface exchange rate of the corresponding cathode. The effect of the powder preparation method on the oxygen bulk diffusion rate of the cathode was also investigated by the oxygen permeation study of the corresponding surface-modified BSCF membranes. A porous layer of BSCF was deposited onto the surface of BSCF membranes exposed to the oxygen-lean side atmosphere. The porous layer resulted in a significant improvement of the effective surface area for oxygen surface exchange; therefore, the importance of oxygen bulk diffusion in the rate determination of the oxygen permeation flux was enhanced. The oxygen permeation fluxes of the surface-modified membranes could then reflect the oxygen bulk diffusion rate. After the surface modification, as shown in Fig. 8, the oxygen permeation flux increased most significantly for the BSCF membrane with the powder prepared by the EC method, followed by the membrane made of NEC-BSCF, while the improvement of the permeation flux of the membrane by NECC-BSCF was the smallest. It suggests that the synthesis techniques also have a significant influence on the bulk oxygen diffusion of the cathode materials. The higher amount of nitric acid applied during the synthesis, the lower oxygen bulk diffusion rate was observed.

The influence of the preparation method on the bulk properties of the BSCF cathode was also supported by the O_2-TPD experiments. Fig. 9 shows the oxygen temperature-programmed desorption curves of EC-BSCF, NEC-BSCF and NECC-BSCF.

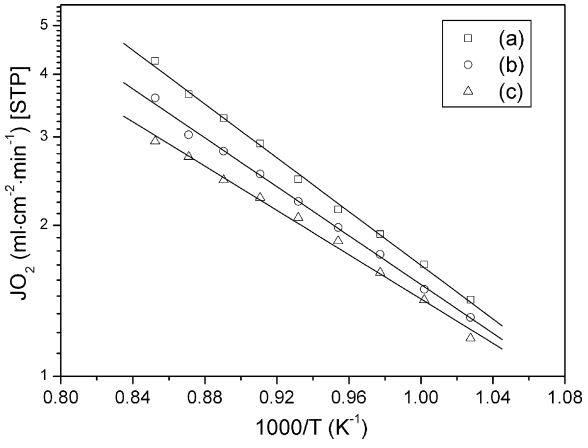

Fig. 8. Arrhenius plots of oxygen permeation fluxes of membranes prepared by (a) EC, (b) NEC and (c) NECC processes with a porous NECC-BSCF layer (~20 μm) at the oxygen-lean side. Membrane thickness: 1 mm; He sweep rate: 100 ml min^{-1}.

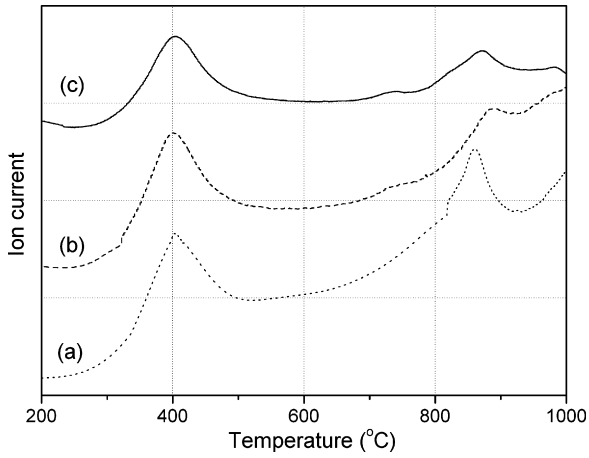

Fig. 9. Oxygen temperature-programmed desorption curves of (a) EC-BSCF, (b) NEC-BSCF and (c) NECC-BSCF.

A significant difference in oxygen desorption behavior at a temperature higher than 800 °C was observed. The oxygen desorption at such a temperature in O_2-TPD profile was associated with the reduction of Co^{3+} to Co^{2+} [47]. The difference in the shape of O_2-TPD profiles for the various BSCF powders suggests that the preparation method has an effect on the cobalt valence state at high temperatures. Since the oxygen bulk diffusion rate is closely related to the oxygen vacancy concentration, which in turn is closely related to the valence state of metal ions in the perovskite structure, a difference in the oxygen bulk diffusion behavior of the various BSCF oxides can be anticipated.

Complete fuel cells were built based on the thin-film SDC electrolyte and the EC-BSCF, NEC-BSCF or NECC-BSCF cathode. Fig. 10 shows the performances of the single cells using 3% water-humidified H_2 as the fuel and ambient air as the cathode atmosphere, operated at 550–650 °C. Peak power densities of 693 and 825 mW cm^{-2} were achieved for the cell with the EC-BSCF cathode at operating temperatures of 600 and 650 °C, respectively. As expected, worse performances were observed for the cells based on the other two cathodes. The peak power densities were only 571 and 543 mW cm^{-2} at 600 °C for cells based on NEC-BSCF and NECC-BSCF cathodes, respectively. Shown in Fig. 11 are the typical impedance spectra for the cells with the EC-BSCF, NEC-BSCF and NECC-BSCF cathodes measured at 600 °C under open circuit condition. Here, the intercept with the real axis at high frequencies represents the resistance of the electrolyte and lead wires (about 0.27 Ω cm^2), whereas the resistance between the two intercepts with the real axis corresponds to the impedance of the two interfaces, i.e. the cathode–electrolyte interface and the anode–electrolyte interface. The electrode ASRs for the cells based on EC-BSCF, NEC-BSCF and NECC-BSCF cathode are 0.067, 0.097 and 0.207 Ω cm^2, respectively. Since the anodes are identical, the differences in the electrode ASRs can be essentially attributed to the cathode. Therefore, it is clear that the interfacial polarization resistance of EC-BSCF cathode was the lowest, which was about 0.03 and 0.14 Ω cm^2 lower than that of NEC-BSCF and NECC-BSCF, respectively.

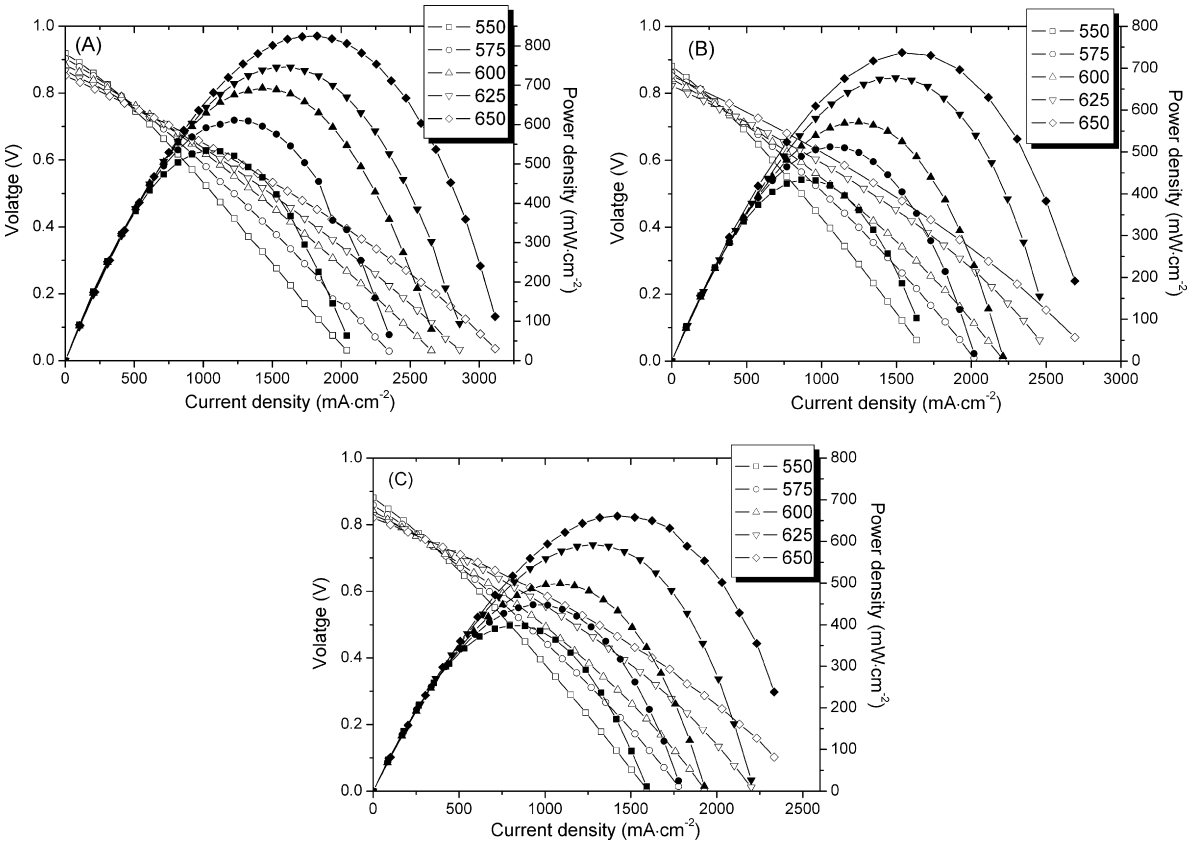

Fig. 10. *I–V* and *I–W* curves of the single cells with the cathode of (A) EC-BSCF, (B) NEC-BSCF and (C) NECC-BSCF.

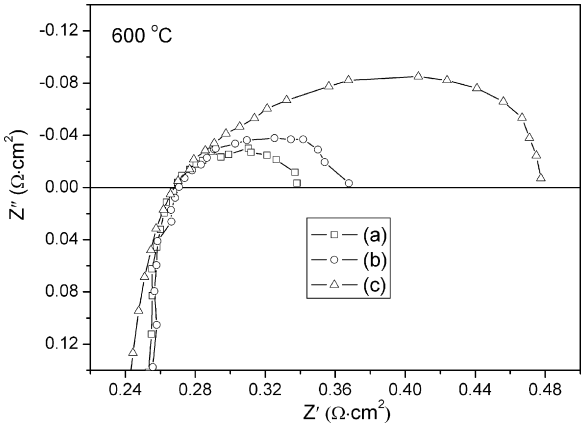

Fig. 11. Impedance spectra for single cells with the cathode operated at 600 °C under OCV condition of (a) EC-BSCF, (b) NEC-BSCF and (c) NECC-BSCF.

4. Conclusions

Synthesis technique has a significant effect on the cathode performance of $Ba_{0.5}Sr_{0.5}Co_{0.8}Fe_{0.2}O_{3-\delta}$ perovskite for solid-oxide fuel cells. The nitric acid treatment during the EDTA–citrate complexing process affects not only the sintering behavior of the cathode during fabrication, but also the oxygen surface exchange kinetics and the oxygen bulk diffusion properties of the cathode. Among the three synthesis methods including the combined EDTA–citrate (EC) complexing method, the nitric acid modified EDTA–citrate (NEC) route and the nitric acid modified EDTA–citrate combustion (NECC) process, the EC method was found to be the most promising one for fuel cell applications. The increase of nitric acid applied during the powder synthesis led to the decrease of the crystallite size of the powder, the increase of sintering during fabrication, and the reduced surface oxygen exchange kinetics and bulk diffusion rate of the cathode. Consequently, the addition of HNO_3 during the synthesis process had a detrimental effect on the performance of fuel cell with the BSCF cathode. Therefore, for advances of IT-SOFCs, besides the development of new cathode materials and the optimization of the cathode architecture, proper powder synthesis techniques of the cathode material is also critical.

Acknowledgements

This work was supported by the National Natural Science Foundation of China under contract Nos. 20646002 and 20676061.

References

[1] B.C.H. Steele, A. Heinzel, Nature 414 (2001) 345.
[2] S.C. Singhal, Solid State Ionics 135 (2000) 305.
[3] D. Hirabayashi, A. Tomita, S. Teranishi, T. Hibino, M. Sano, Solid State Ionics 176 (2005) 881.
[4] M.J.L. Ostergard, C. Clausen, C. Bagger, M. Mogensen, Electrochim. Acta 40 (1994) 1971.
[5] T. Hibino, A. Hashimoto, T. Inoue, J. Tokuno, S. Yoshida, M. Sano, Science 288 (2000) 2031.

[6] P. Holtappels, C. Bagger, J. Eur. Ceram. Soc. 22 (2002) 41.
[7] E.P. Murray, S.A. Barnett, Solid State Ionics 143 (2001) 265.
[8] C. Xia, L. Yang, G. Meng, Fuel Cells 4 (2004) 41.
[9] P. Holtappels, U. Vogtand, T. Graule, Adv. Eng. Mater. 7 (2005) 292.
[10] D. Beckel, U.P. Muecke, T. Gyger, G. Florey, A. Infortuna, L.J. Gauckler, Solid State Ionics 178 (2007) 407.
[11] S.Z. Wang, H. Zhong, J. Power Sources 165 (2007) 58.
[12] C.R. Xia, M.L. Liu, Solid State Ionics 144 (2001) 249.
[13] X. Zhang, M. Robertson, S. Yick, C. Deĉes-Petit, E. Styles, W. Qu, Y. Xie, R. Hui, J. Roller, O. Kesler, R. Maric, D. Ghosh, J. Power Sources 160 (2006) 1211.
[14] V. Dusastre, J.A. Kilner, Solid State Ionics 126 (1999) 163.
[15] J.D. Zhang, Y. Ji, H.B. Gao, T.M. He, J. Liu, J. Alloys Compd. 395 (2005) 322.
[16] H.J. Hwang, J.-W. Moon, S. Lee, E.A. Lee, J. Power Sources 145 (2005) 243.
[17] Y.L. Zhang, S.W. Zha, M.L. Liu, Adv. Mater. 17 (2005) 487.
[18] M.G. Bellino, J.G. Sacanell, D.G. Lamas, A.G. Leyva, N.E. Walsoe de Reca, J. Am. Chem. Soc. 129 (2007) 3066.
[19] J.C. Ruiz-Morales, J. Canales-Vázquez, J. Peña-Martínez, D. Marrero-López, J.T.S. Irvine, P. Núñez, J. Mater. Chem. 16 (2006) 540.
[20] M. Sadakane, T. Asanuma, J. Kubo, W. Ueda, Chem. Mater. 17 (2005) 3546.
[21] M. Gaudon, C. Laberty-Robert, F. Ansart, L. Dessemond, P. Stevens, J. Power Sources 133 (2004) 214.
[22] K.T. Lee, A. Manthiram, J. Power Sources 158 (2006) 1202.
[23] A. Tarancón, G. Dezanneau, J. Arbiol, F. Peiró, J.R. Morante, J. Power Sources 118 (2003) 256.
[24] N.P. Bansal, Z.M. Zhong, J. Power Sources 158 (2006) 148.
[25] L. Ge, W. Zhou, R. Ran, Z. P. Shao, S. M. Liu, J. Alloys Compd., doi:10.1016/j.jallcom.2006.10.142.
[26] R.J. Bell, G.J. Millar, J. Drennan, Solid State Ionics 131 (2000) 211.
[27] S. Royer, F. Bérubé, S. Kaliaguine, Appl. Catal. A 282 (2005) 273.
[28] X. Zhu, Y. Cong, W. Yang, J. Membr. Sci. 283 (2006) 158.
[29] J. Sfeir, S. Vaucher, P. Holtappels, U. Vogt, H.-J. Schindler, J. Van herle, E. Suvorova, P. Buffat, D. Perret, N. Xanthopoulos, O. Bucheli, J. Eur. Ceram. Soc. 25 (2005) 1991.
[30] L. Tan, X. Gu, L. Yang, W. Jin, L. Zhang, N. Xu, J. Membr. Sci. 212 (2003) 157.
[31] L. Yang, Z.T. Wu, W.Q. Jin, N.P. Xu, Ind. Eng. Chem. Res. 43 (2004) 2747.
[32] Z.T. Wu, W. Zhou, W.Q. Jin, N.P. Xu, AIChE J. 52 (2006) 769.
[33] Z.P. Shao, S.M. Haile, Nature 431 (2004) 170.
[34] Z.P. Shao, S.M. Haile, J. Ahn, P.D. Ronney, Z.L. Zhan, S.A. Barnett, Nature 435 (2005) 795.
[35] W. Zhou, Z.P. Shao, R. Ran, Z.H. Chen, P.Y. Zeng, H.X. Gu, W.Q. Jin, N.P. Xu, Electrochim. Acta 52 (2007) 6297.
[36] W. Zhou, Z.P. Shao, R. Ran, P.Y. Zeng, H.X. Gu, W.Q. Jin, N.P. Xu, J Power Sources 168 (2007) 330.
[37] Y. Zhang, X. Huang, Z. Lu, Z. Liu, X. Ge, J. Xu, X. Xin, X. Sha, W. Su, J. Power Sources 160 (2006) 1217.
[38] Z. Duan, M. Yang, A. Yan, Z. Hou, Y. Dong, Y. Chong, M. Cheng, W. Yang, J. Power Sources 160 (2006) 57.
[39] Q.L. Liu, K.A. Khor, S.H. Chan, J. Power Sources 161 (2006) 123.
[40] J. Peña-Martínez, D. Marrero-López, J.C. Ruiz-Morales, B.E. Buergler, P. Núñez, L.J. Gauckler, Solid State Ionics 177 (2006) 2143.
[41] W. Zhou, Z.P. Shao, W.Q. Jin, J. Alloys Compd. 426 (2006) 368.
[42] W. Zhou, X.P. Xue, L. Ge, Y. Zheng, Z.P. Shao, W.Q. Jin, J. Inorg. Mater. 22 (2007) 657.
[43] W. Zhou, Z.P. Shao, W.Q. Jin, Chin. Chem. Lett. 17 (2006) 1353.
[44] A. Subramania, T. Saradha, S. Muzhumathi, J. Power Sources 165 (2007) 728.
[45] B. W. Liu, Y. Zhang, J. Alloys Compd., doi:10.1016/j.jallcom.2006.11.142.
[46] P.Y. Zeng, Z.H. Chen, W. Zhou, H.X. Gu, Z.P. Shao, S.M. Liu, J. Membr. Sci. 291 (2007) 148.
[47] Z.P. Shao, W.S. Yang, Y. Cong, H. Dong, J.H. Tong, G.X. Xiong, J. Membr. Sci. 172 (2000) 177.